Journal of Controlled Release 342 (2022) 1–13

Contents lists available at ScienceDirect

Journal of Controlled Release

journal homepage: www.elsevier.com/locate/jconrel

Dual-modified nanoparticles overcome sequential absorption barriers for oral insulin delivery

Ziyue Xi [a,b,1], Ejaj Ahmad [a,1], Wei Zhang [b], Jingyi Li [a], Aohua Wang [a,c], Faridoon [c,d], Ning Wang [a,c], Chunliu Zhu [a], Wei Huang [c,d], Lu Xu [b,*], Miaorong Yu [a,*], Yong Gan [a,c,e,**]

[a] State Key Laboratory of Drug Research, Shanghai Institute of Materia Medica, Chinese Academy of Sciences, Shanghai 201203, China
[b] School of Pharmacy, Shenyang Pharmaceutical University, Shenyang 110016, China
[c] University of Chinese Academy of Sciences, No. 19A Yuquan Road, Beijing 100049, China
[d] CAS Key Laboratory of Receptor Research, CAS Center for Excellence in Molecular Cell Science, Shanghai Institute of Materia Medica, Shanghai 201203, China
[e] NMPA Key Laboratory for Quality Research and Evaluation of Pharmaceutical Excipients, National Institutes for Food and Drug Control, Beijing 100050, China

ARTICLE INFO

Keywords:
Absorption barriers
Sequential delivery
Transcytosis
Intracellular trafficking
Insulin

ABSTRACT

The efficacy of oral insulin drug delivery is seriously hampered by multiple gastrointestinal barriers, especially transepithelial barriers, including apical endocytosis, lysosomal degradation, cytosolic diffusion and basolateral exocytosis. In this study, a functional nanoparticle (PG-FAPEP) with dual-modification was constructed to sequentially address these important absorption obstacles for improved oral insulin delivery. The dual surface decorations folate and charge-convertible tripeptide endowed PG-FAPEP with the ability to target the apical and basolateral sides of enterocytes, respectively. After fast diffusion across the mucus layer, PG-FAPEP could be efficiently internalized into epithelial cells *via* a folate receptor-mediated pathway and subsequently became positively charged in acidic lysosomes due to the surface tripeptide, triggering the proton sponge effect to escape lysosomes. When entering the cytosolic medium, PG-FAPEP was converted to neutral charge again, attenuating intracellular adhesion, and gained improved motility toward the basolateral side. Finally, the tripeptide helped PG-FAPEP recognize the proton-coupled oligopeptide transporter (PHT1) in the basolateral membrane, boosting intact exocytosis across intestinal epithelial cells. The *in vivo* studies further verified that PG-FAPEP could traverse the intestinal epithelium by folate receptor-mediated endocytosis, lysosomal escape, and PHT1-mediated exocytosis, exhibiting a high oral insulin bioavailability of 14.3% and a prolonged hypoglycemic effect. This formulation addresses multiple absorption barriers on demand with a simple dual-modification strategy. Therefore, these features allow PG-FAPEP to unleash the potential of oral macromolecule delivery.

1. Introduction

Long hailed as the 'Holy Grail' of drug delivery, oral insulin offers great potential but also presents considerable challenges [1–3]. The sequential barriers in the gastrointestinal tract, including the harsh pH environment, enzymes, mucus and intestinal epithelium, stand as severe obstacles limiting insulin absorption [4,5]. In recent decades, nanoparticles (NPs), which can inherently protect entrapped drugs against acidic denaturation and enzymatic degradation, have been extensively exploited to promote oral insulin absorption [6–8]. A diverse range of strategies that optimize particle physicochemical properties, such as size, shape, and surface modification, have been thoroughly explored to facilitate mucus penetration and augment cellular uptake [9–11]. However, restricted intracellular trafficking and inefficient exocytosis on the basolateral side are still difficult issues to address. To fully realize the therapeutic effect of oral insulin, NPs must traverse through the intestine and enter the blood circulation. Recent studies have revealed that the internalized amount of drug and NPs in enterocytes is usually much higher than the transepithelial amount, offering strong evidence that challenges still persist [12–15]. Therefore, conquering the sequential absorption barriers step by step, especially the transepithelial barriers, is of great importance to facilitate efficacious oral insulin

* Corresponding authors.
** Corresponding author at: State Key Laboratory of Drug Research, Shanghai Institute of Materia Medica, Chinese Academy of Sciences, Shanghai 201203, China.
E-mail addresses: xulu@syphu.edu.cn (L. Xu), mryu@simm.ac.cn (M. Yu), ygan@simm.ac.cn (Y. Gan).
[1] These authors contributed equally to this work.

https://doi.org/10.1016/j.jconrel.2021.11.045
Received 28 August 2021; Received in revised form 24 November 2021; Accepted 29 November 2021
Available online 2 December 2021

delivery.

All transepithelial delivery processes include apical endocytosis, lysosomal escape, cytosolic diffusion and basolateral exocytosis. Although apical internalization can be easily improved by modifying NPs [16–19], it is difficult to manipulate the intracellular delivery of NPs. After cellular uptake, NPs are always transported into lysosomal compartments, followed by the degradation of loaded insulin molecules inside lysosomes. Engineering NPs to escape lysosomes using the proton sponge mechanism holds potential to address this issue [20–22]. However, it should be noted that the cytosol is another major barrier preventing intracellular trafficking. The cytosolic medium, which consists of myriad proteins, cytoskeleton, and organelles, forms a negatively charged and adhesive mesh structure restricting the diffusion of lysosome-escaping NPs toward the basolateral side. State-of-the-art studies have revealed that NPs with neutrally charged surfaces can freely penetrate biological hydrogels such as the cytoplasm [23–25]. Finally, the basolateral membrane poses a barrier hindering the transport of therapeutics from the cell to the circulation. To date, the comprehensive picture of basolateral exocytosis for NPs, including basolateral recognition and release into blood circulation, remains mysterious. As a result, orally administered NPs exhibit low transcytosis efficiency, thus limiting the efficacy of oral insulin absorption.

The polarity of intestinal epithelial cells may provide pivotal clues for the rational design of NPs with unidirectional transport capacity from the apical side to the basolateral side, thus sequentially passing multiple absorption barriers. Transport proteins, which provide targets for ligand-modified NPs, are usually asymmetrically distributed in the apical and basolateral membranes of epithelial cells [26]. This means that NPs that successively recognize apical and basolateral transport proteins might traffic from the apical side to the basolateral side for efficient transcytosis. The folate receptor, which has been widely investigated to improve apical endocytosis, is an ideal target for apical recognition [27,28]. On the basolateral side of intestinal epithelial cells, proton-coupled oligopeptide transporter (PHT1), which can transfer peptides and amino acids across the basolateral membrane to the bloodstream [29,30], is another important target. Recently, researchers have revealed that transporters, such as bile acid transporter [15,31], and Na^+-coupled absorption transporter OCTN2 (SLC22A5) [32], are involved in the transportation of nanoparticles across membrane to increase oral bioavailability [33]. These findings further suggest the potential of targeting PHT1 for oral drug delivery. Therefore, we hypothesize that dual-ligand modification to enable separate binding to the apical folate receptor and basolateral PHT1 might accelerate the transcytosis of NPs across the intestinal epithelium.

Herein, we developed a functional NP (PG-FAPEP) modified with dual targeting moieties to negotiate sequential absorption barriers. The underlying transport pathway of PG-FAPEP across the gastrointestinal tract is illustrated in Scheme 1. Specifically, we introduced folate to target folate receptors in the apical membrane for enhanced apical endocytosis and designed a tripeptide to recognize basolateral PHT1 for efficient exocytosis from the basolateral side into the bloodstream. In addition, due to the pH-responsive charge conversion capacity, the tripeptide endowed PG-FAPEP with superior mucus diffusion, enhanced lysosome-escaping capacities and accelerated motion in the cytoplasm. In summary, PG-FAPEP obtained the ability to successively overcome multiple gastrointestinal obstacles step by step, achieving a high oral bioavailability of insulin in diabetic rats. Therefore, this strategy we developed to overcome sequential absorption barriers is a promising approach to solve the overwhelming challenges of oral protein drugs.

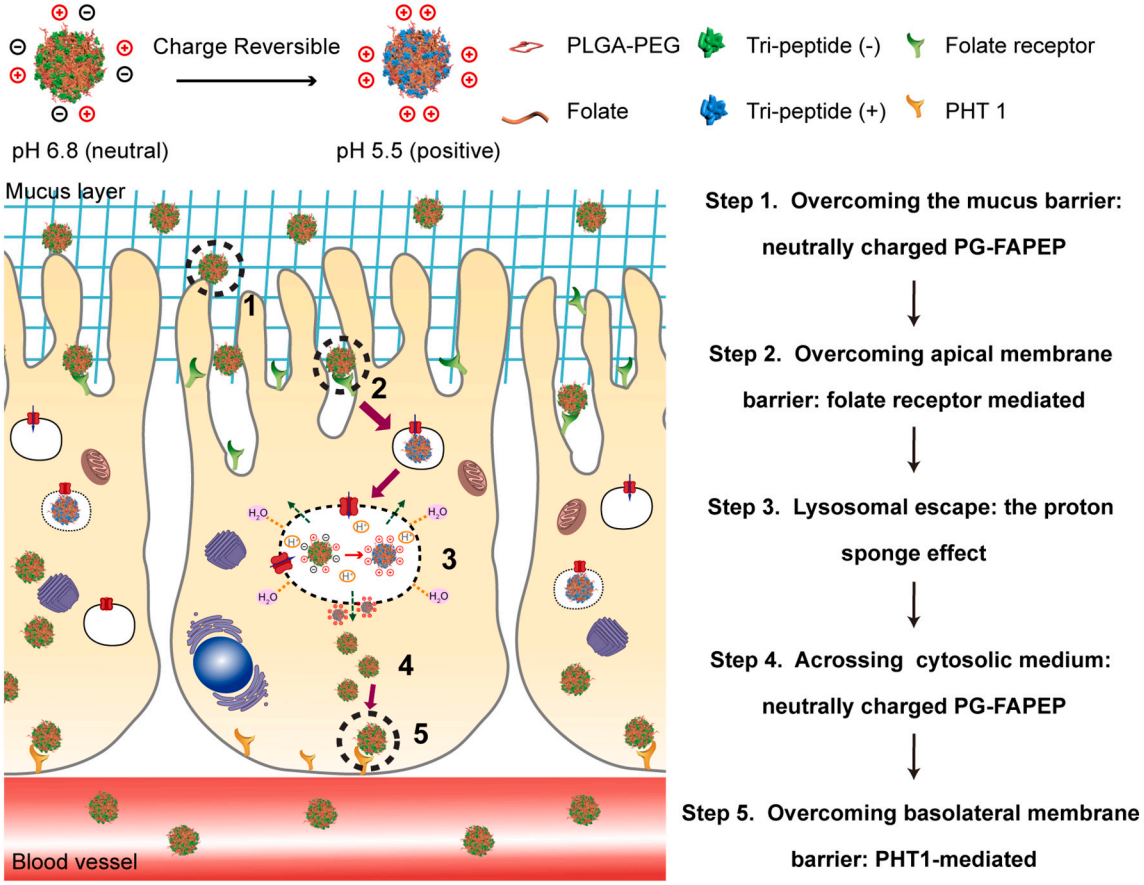

Scheme 1. Schematic representation of the composition of multifunctional NPs (PG-FAPEP) and the pathway to overcome the sequential absorption barriers.

2. Materials and methods

2.1. Materials, cell lines and animals

Folate, N-hydroxysuccinamide (NHS) and dicyclohexylcarbodiimide (DCC) were obtained from Sigma Aldrich (St Louis, MO, USA). PEG-bis-amine (H_2N-PEG-NH_2, MW 2000 Da), PLGA-COOH (PLGA 50:50, MW 5000 Da), triethylamine (Et_3N), anhydrous DMSO, and anhydrous CH_2Cl_2 were purchased from Aladdin Reagent Co., Ltd. (Shanghai City, China). Human insulin was purchased from Shanghai Hao Sheng Biological Technology Co., Ltd. Transwell® inserts were purchased from Corning (New York, USA). Human insulin ELISA kits were purchased from Mercodia (Uppsala, Sweden). Brefeldin A (BFA), histidine (His), LysoTracker DND, bafilomycin A1, and 5(6)-fluorescein isothiocyanate (FITC) were purchased from Dalian Meilun Company. Lysosomal-associated membrane protein 1 (LAMP1) rabbit mAb were obtained from Cell Signaling Technology. RIPA lysis buffer, anti-mouse secondary IgG Alexa Fluor 647 antibody and 2-(4-amidinophenyl)-6-indolecarbamidine dihydrochloride (DAPI) were purchased from Beyotime (Jiangsu, China). SLC15A4 antibody was purchased from Shanghai Duma Biotechnology Company, and anti-rabbit secondary IgG Alexa Fluor 647 antibody was purchased from Abcam. Streptozotocin (STZ) was purchased from Shanghai Yeasen Company. PCcaps™ capsules were purchased from Suzhou Capsugel Company (Suzhou, China). Hydroxypropyl methylcellulose phthalate (HPMCP, Mw = ~45,000) was purchased from Acros Organics Company (Belgium, USA). All other reagents were purchased from Sinopharm Chemical Reagent Co., Ltd. (Shanghai, China).

Caco-2 cells were obtained from American Type Culture Collection (ATCC, Manassas, VA, USA), and HT29-MTX-E12 (E12) cells were supplied by the ADME Department of Novo Nordisk. Male Sprague-Dawley (SD) rats (200 ± 20 g) were obtained from the Animal Experiment Center of Shanghai Institute of Materia Medica.

All animal experiments were conducted according to Institutional Animal Care and Use Committee (IACUC, 2019–12-GY-55) guidelines. For the induction of diabetes, the rats were intraperitoneally injected with STZ solution (65 mg/kg) dissolved in citrate buffer (pH 4.5) as previously described [34].

2.2. Synthesis and characterization of functionalized polymers

2.2.1. Synthesis of PLGA-PEG-NH_2 and PLGA-PEG-FA conjugates

Amine-terminated di-block copolymer (PLGA-PEG-NH_2) was synthesized with slight modifications of a previously reported method [35]. Briefly, PLGA-COOH (200 mg) was mixed with DCC (16 mg) and NHS (11.5 mg) under a N_2 atmosphere, and then the above mixture was added to PEG-bis-amine solution with gentle stirring to obtain PLGA-PEG-NH_2. To synthesize PLGA-PEG-FA, PLGA-PEG-NH_2 was mixed with folate, N,N′-dicyclohexylcarbodiimide and triethylamine and allowed to react for 8 h. The crude extract of PLGA-PEG-FA was dissolved in dichloromethane (DCM), and the unconjugated folate was further removed by filtration.

2.2.2. Characterization of PLGA-PEG-FA by ^1H NMR and FTIR

The purified PLGA-PEG-FA was dissolved in DMSO, and the polymer content of the solution was analyzed by ultraviolet spectroscopy at 365 nm. Then, the prepared PLGA-PEG-FA was dissolved in deuterated DMSO, and its structure was characterized using ^1H NMR. The spectrum was recorded at 298 K on a Varian Inova 500 MHz spectrometer (Agilent Technologies, Santa Clara, CA, USA). To further confirm the structure of the polymers, PLGA-PEG-FA was dissolved in DCM and analyzed by FTIR (Nicolet Impact 410, Perkin Elmer Instrument, MA, USA).

2.2.3. Synthesis and characterization of PLGA-PEG-PEP conjugates

PLGA-PEG-NH_2 and DCC were dissolved in anhydrous DCM, and the synthesized tripeptide (method in Supporting Information) and Et_3N were added to the DCM solution. The mixture was dialyzed to remove unconjugated tripeptide and finally lyophilized into powder (denoted as PLGA-PEG-PEP) and stored at 254 K for subsequent use. The structure of PLGA-PEG-PEP was also characterized by ^1H NMR and FTIR, and the relative spectra were recorded.

2.3. Preparation and characterization of NPs

NPs including PLGA NPs (PG), folate-modified PLGA NPs (PG-FA), tripeptide-modified PLGA NPs (PG-PEP), and folate and tripeptide dual-modified PLGA NPs (PG-FAPEP) were prepared using a previously reported self-assembly method [36]. Polymers were dissolved in DMSO, and then the organic solution was dropped into water with magnetic stirring to obtain NPs. The NP surfaces were modified with equal amounts of folate or tripeptide (Table S1). The morphology of NPs was characterized using a Tecnai 12 electron microscope (TEM). Samples were added dropwise onto a carbon-coated copper grid and prepared in a Vitrobot (FEI). The imaging was carried out at approximately 90 K. The TEM instrument was operated at an accelerated voltage of 200 kV. The synthesized PG-FAPEP was incubated with simulated intestinal fluid (SIF) to evaluate its stability at predetermined intervals using FRET spectra.

2.4. Buffering capacity of the copolymer conjugates and NPs

The buffering capacity of conjugates and NPs was determined by following a published procedure [37]. Polymer conjugates (3 mg/mL) and NPs (0.3 mg/mL) were separately dissolved in 0.01 M NaOH solution (pH 11.0). Subsequently, these solutions were dropped into the 0.01 M HCl to perform the titrated experiment, and the changes in pH were recorded. A normal saline group was used as a control.

2.5. Multiple particle tracking

In this study, native intestinal mucus was collected from the gastrointestinal tracts of healthy rats and equilibrated for 15 min (37 °C) to guarantee homogeneous dispersion. FITC-labeled NPs were incubated with a mucus mixture for another 30 min at 37 °C. Fluorescence microscopy (DMI 4000B, Leica, Germany) was utilized to capture movies at a temporal resolution of 32.6 ms for 10 s. The obtained data were analyzed using Fiji/ImageJ software. The time-averaged mean square displacement (MSD) and effective diffusivities (D_{eff}) were calculated as follows:

$$MSD_\tau = \left(x_{(t+\tau)} - x_t\right)^2 + \left(y_{(t+\tau)} - y_t\right)^2 \quad (1)$$

$$D_{eff} = MSD/(4\tau) \quad (2)$$

(where x and y represent the coordinates of the particles, and τ is the time scale)

2.6. Apical endocytosis of NPs

2.6.1. Apical endocytosis of NPs on Caco-2 and E12 cells

Caco-2 cell viability was measured by methyl tetrazolium (MTT) assay at the tested concentrations of NPs (0– 500 μg/mL). To evaluate the apical endocytosis of prepared NPs quantitatively, Caco-2 and E12 cells were incubated with FITC-labeled NPs (125 μg/mL) for 1 h. Cells were treated with RIPA lysis solution, and the cell suspensions were collected and further analyzed by a bicinchoninic acid (BCA) protein assay kit. Quantitative fluorescence analysis was performed at 530/565 nm (excitation/emission) using a Synergy H1m microplate reader.

Similarly, both E12 and Caco-2 cells were incubated with FITC-labeled NPs and fixed in 4% paraformaldehyde for further intuitive observation of endocytosis. Then, nuclei were stained with DAPI, and fluorescent images were obtained by confocal laser scanning microscopy

(CLSM, FV1000, Olympus).

2.6.2. Mechanism of apical endocytosis

The endocytosis mechanism of NPs was studied using a published method [16]. Briefly, Caco-2 cells and NPs were coincubated following pretreatment with different endocytic inhibitors, including folate (20 μM) and tripeptide (20 μM), for 1 h. Afterwards, nuclei were stained with DAPI and mounted on microscope slides to be observed under CLSM.

2.7. Intracellular trafficking and exocytosis of NPs

2.7.1. Lysosomal escape of NPs

An intracellular trafficking study was performed using a published procedure [22]. Briefly, lysosomes were labeled with LysoTracker DND (red) and incubated with FITC-labeled NPs for 0.5 and 2 h. Cell samples were then stained with DAPI and observed by CLSM. The NPs were quantitatively analyzed by Fiji/ImageJ software. To investigate the mechanism of lysosomal escape in epithelial cells, Caco-2 cells were pretreated with bafilomycin A1 for 1 h before the addition of NPs, and the colocalization M value was evaluated by Fiji/ImageJ software. Moreover, to confirm lysosomal escape at the organizational level, an intracellular trafficking study was performed in the small intestinal villi of rats. FITC-labeled NPs were injected into the small intestine and incubated for 2 h. Finally, the intestinal segments of rats were sliced, and lysosomes were stained with LAMP1 rabbit mAb (red) overnight prior to treatment with anti-rabbit secondary IgG Alexa Fluor 647 antibody. Cell samples were then stained with DAPI and observed by CLSM.

2.7.2. NP diffusion across cytoplasm

To further describe the transport velocity of NPs in the viscous cytoplasm, *in vitro* tracking experiments in the intracellular cytoplasm were conducted as previously reported [24]. To simulate the cytoplasm, 0.2% hydroxyethyl cellulose was selected as the medium. Two microliters of NPs, PG and PG-FAPEP (200 μg/mL), were mixed with 100 μL of medium and then coincubated at 37 °C for 10 min. Movies were captured for approximately 10 s by an inverted fluorescence microscope, and the movies were analyzed by Fiji/ImageJ software. The time-averaged mean square displacement (MSD) and effective diffusivities (D_{eff}) were calculated as the intracellular diffusion of NPs.

2.7.3. Transepithelial transport

Caco-2 cells were cultured (5×10^4 cells/well) on polycarbonate membranes (pore size: 0.4 μm) in Transwells (Corning Costar Corp). The integrity of cell monolayers was monitored by measuring the transepithelial electrical resistance (TEER) with an electrical resistance meter (Milli cell ERS-2, Millipore). Monolayers with TEER values >300 Ω × cm^2 were used in the experiments. First, the apical solutions were diluted with HBSS to a final particle concentration of 125 μg/mL. At various time points, the TEER values were measured, and the P_{app} values were calculated as follows:

$$P_{app} = \frac{dQ}{dt} \times \frac{1}{A \times C_0} \quad (3)$$

where dQ/dt is the slope of the linear relationship between the cumulative amounts of insulin transported *vs.* time, C_0 is the initial concentration of FITC-insulin encapsulated into NPs in the donor compartment, and A is the area (cm^2) of the membrane. The transcellular efficiency of NP transport from the apical side to the basolateral side was calculated according to the transported amounts of insulin and the values of drug loading capacity.

The proton-coupled oligopeptide transporter (PHT1) has been reported to be located on the basolateral side, which is crucial for transcytosis from the basolateral side to the systematic circulation To reveal the exocytosis mechanism of PG-FAPEP, the cell monolayers were pretreated with histidine (His, a specific competitive substrate for PHT1), and the P_{app} values were then determined as described above.

2.7.4. Basolateral exocytosis of NPs

FITC- and RITC-labeled NPs were added to the donor compartment of the Transwells and incubated with the cell monolayers for 2 h. The collected sample on the basolateral side was then removed and measured by cryo-TEM and a Synergy H1m microplate reader. The same volume of HBSS was added to the acceptor compartment. The FRET spectra were recorded with an excitation wavelength of 420 nm and emission wavelengths in the range of 450–700 nm.

To further clarify the detailed mechanism of exocytosis for PG-FAPEP, cell monolayers and small intestinal villi slides were then observed under CLSM. Both the Caco-2 cell monolayer and intestinal villi slides were incubated with FITC-labeled NPs for 1 h and fixed with 4% paraformaldehyde for 30 min at 25 °C. Then, immune fluorescent staining of PHT1 was performed. First, cell monolayers were incubated with the blocking solution (1% BSA in PBS with 0.3% Triton X-100) for 1 h. After discarding the blocking solution, cell monolayers were incubated overnight at 4 °C with SLC15A4 antibody and incubated with anti-rabbit secondary IgG Alexa Fluor 647 antibody for 1 h. Afterwards, the membranes were mounted on microscope slides and stained with DAPI. The data were analyzed by LAS X and Bitplane Imaris 7.2.3.

2.8. Intravital two-photon microscopy studies

Intravital two-photon microscopy studies were conducted as previously reported [15]. Briefly, diabetic rats were fasted overnight before dosing and with free access to water. The nuclei were stained by intraperitoneal injection of Hoechst 33258 (2 mg/kg), and the rats were then anesthetized with urethane. A small incision was made to expose the intestine and open the jejunum along the central axis. The jejunum section was then attached to the bottom of the glass culture dish. FITC-insulin-loaded NPs were dropped on the jejunum section, and time-lapse images were obtained by two-photon microscopy (Olympus FV1200PE) with a water-immersed 25× objective. In addition, 20 μM free folate and free peptide were added as inhibitors. The data were analyzed by FV10-ASW 4.2 Viewer and Bitplane Imaris 7.2.3.

2.9. Hypoglycemic effect and pharmacokinetic study

The insulin-loaded PLGA NPs were freeze-dried with 2% trehalose as a cryoprotectant and filled into the capsules according to the dose standard of 45 IU/kg. NP-filled capsules were immersed in HPMCP solution (40 mg/mL, solvent mixture of 80% dichloromethane, 20% acetone) and then air-dried at room temperature (298 K). The above procedure was repeated three times to obtain enteric-coated capsules. HPMCP-coated capsules composed of insulin-loaded PG, PG-FA, PG-PEP and PG-FAPEP were denoted by cPG, cPG-FA, cPG-PEP and cPG-FAPEP, respectively.

Diabetic animals were fasted overnight with free access to water before experiments. Animals were administered intragastrically insulin-loaded NPs in HPMCP-coated capsules at a dose of 45 IU/kg. Subcutaneous injection (s.c.) of insulin solution (5 IU/kg, denoted as INS) and oral administration of HPMCP-coated capsules loaded with trehalose (denoted as cINS) were used as controls [38–40]. Blood glucose levels were measured at predetermined time intervals. For plasma insulin level analysis, blood samples were collected at various time points, and plasma was obtained by centrifuging the available samples at 1800 × g for 5 min. The concentration of insulin was quantified using a human insulin ELISA kit (R&D System, Inc.) and the area under the curve (AUC) of plasma insulin concentration *vs.* time was calculated. The relative bioavailability (F%) of the tested NPs after administration was calculated as follows:

$$F(\%) = \frac{AUC_{oral} \times Dose_{s.c.}}{AUC_{s.c.} \times Dose_{oral}} \quad (4)$$

2.10. Statistical analysis

All experiments were performed in triplicate if there was no special statement. Two-tailed Student's *t*-test was conducted to compare two groups, and one-way ANOVA was selected when comparing multiple groups. p is considered statistically significant as $^{*}p < 0.05$; $^{**}p < 0.01$; $^{***}p < 0.001$ and $^{****}p < 0.0001$.

3. Results and discussion

3.1. Synthesis and characterization of functionalized PLGA-based conjugates

For the preparation of functional NPs, PLGA-related conjugates, including PLGA-PEG-FA and PLGA-PEG-PEP, were selected as original materials. First, we designed a charge-convertible tripeptide (Figs. S1-S4). PLGA-PEG-FA and PLGA-PEG-PEP were then obtained by the conjugation of PLGA-PEG-NH_2 with folate or tripeptide, respectively, *via* covalent amide reactions (Fig. 1A). ^{1}H NMR spectroscopy was performed to confirm the exact structure of the synthesized conjugates (Fig. 1B). The marked signals were attributed to the characteristic peaks of PLGA-PEG-FA and PLGA-PEG-PEP. Fourier transform infrared spectroscopy (FTIR) was further performed to identify the characteristic functional groups in PLGA-PEG-FA and PLGA-PEG-PEP. The stretching and bending vibrations of amine (N—H) bond frequencies were observed at ~3400 cm^{-1} and ~ 1552 cm^{-1}, and the C—N absorption band was shown at ~1252 cm^{-1}, which might be evidence for amide bond formation between PLGA and PEG (Fig. 1C). In addition, the presence of C—H stretching of the benzene ring at ~800 cm^{-1} and C═C bending of the aromatic ring in folate at ~1580 cm^{-1} confirmed that folate had conjugated with the copolymer. The presence of aromatic

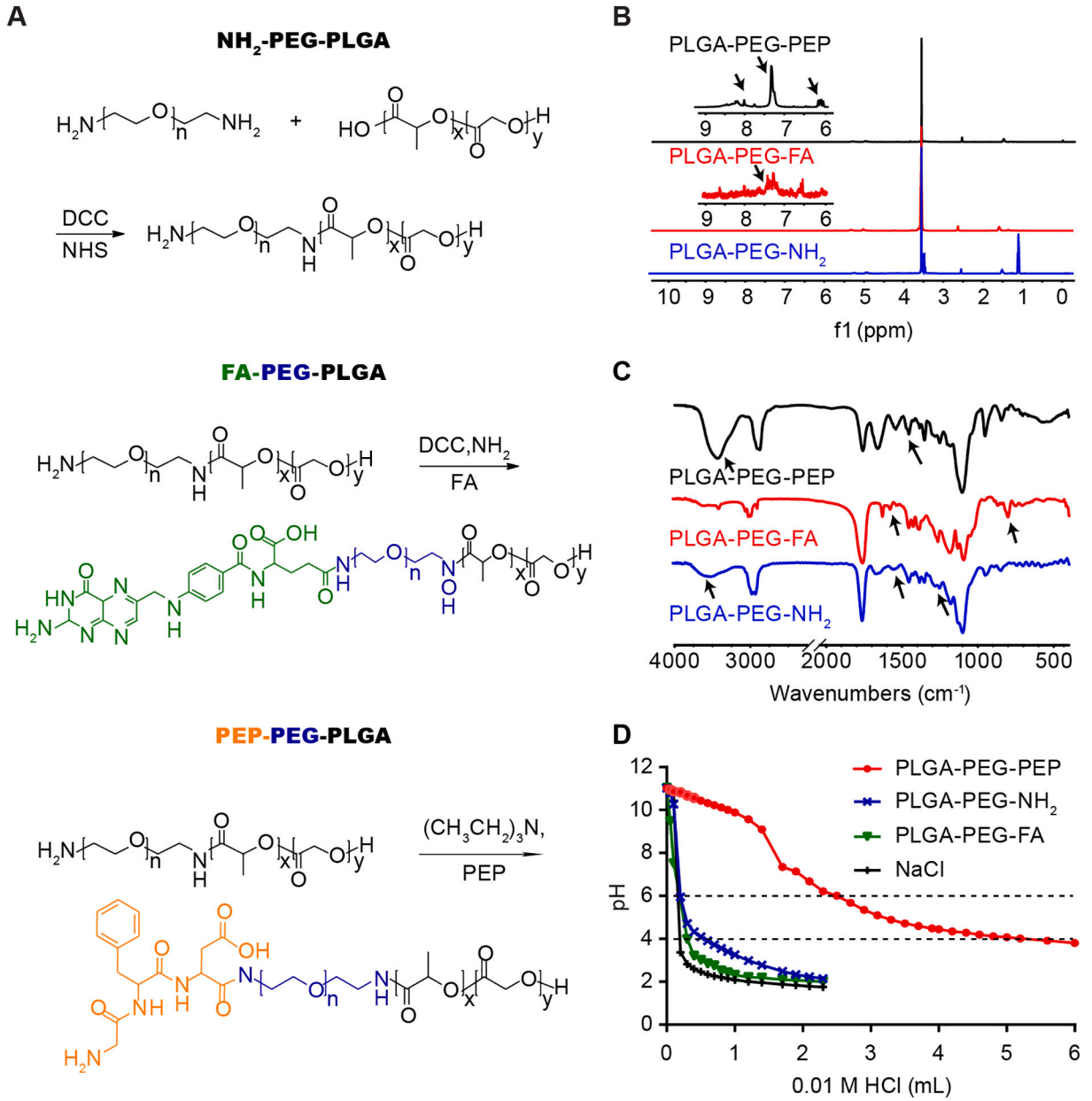

Fig. 1. Synthesis and characterization of functionalized PLGA conjugates. (A) Synthetic procedures, (B) ^{1}H NMR spectra, and (C) FTIR spectra of PLGA-PEG-NH_2, PLGA-PEG-FA and PLGA-PEG-PEP. (D) Titration curves of PLGA-PEG-NH_2, PLGA-PEG-FA and PLGA-PEG-PEP solutions. NaCl solution was used as the control.

C═C and carboxyl OH stretching frequencies at ~1455 cm^{-1} and ~ 3430 cm^{-1}, respectively, confirmed the successful conjugation of PLGA-PEG-PEP. The quantitative percentages of folate and peptide modifications were 33.0 ± 2.5 mol% and 34.0 ± 2.0 mol%, respectively.

3.2. Buffering capacity of PLGA-PEG-PEP polymer

It has been reported that materials with a high buffering capacity can induce proton sponge effects through protonation and deprotonation to help particles escape lysosomes [41]. Herein, an acid-base titration experiment was performed to investigate the buffering capacities of all the conjugates (PLGA-PEG-PEP, PLGA-PEG-FA and PLGA-PEG-NH_2). As shown in Fig. 1D, the pH values gradually decreased with the addition of HCl to the polymer solutions. For the PLGA-PEG-PEP group, a larger volume of HCl was needed when the pH was changed from 4.0 to 6.0, and it was 9.0-fold higher than that for the other groups, indicating the excellent intrinsic buffering capacity of PLGA-PEG-PEP. Thus, we speculate that the modification of tripeptides could trigger sponge effects and further help NPs escape lysosomes (pH 5.5).

3.3. Preparation and characterization of the functionalized NPs

Particles approximately 100 nm in diameter have been reported to show superior oral delivery efficacy [42]. Herein, NPs with a hydrodynamic diameter of approximately 100 nm were fabricated as follows: PLGA NPs (PG), folate-modified PLGA NPs (PG-FA), tripeptide-modified PLGA NPs (PG-PEP), and folate and tripeptide dual-modified PLGA NPs (PG-FAPEP) (Table S2). Cryo-TEM showed that all the NPs were spherical (Fig. 2A), and their sizes were consistent with the hydrodynamic diameters. To investigate the stability of the synthesized NPs in simulated intestinal fluid (SIF), size measurements and radiometric fluorescence resonance energy transfer (FRET) analysis were employed. As shown in Fig. S5, the size and PDI of each NP group changed slightly after incubation with SIF, indicating the stability of the NPs. The FRET studies also confirmed that PG-FAPEP was intact in SIF during the incubation periods (Fig. 2B and C). The loading capacity of insulin in each NP was approximately 10% (Table S1). And the release profile of insulin-loading NPs (PG, PG-FA, PG-PEP, and PG-FAPEP) in SGF and SIF was evaluated *in vitro*. The results showed that approximately 20–45% of the insulin was released from the NPs within 8 h (Fig. S6).

The buffering capacity of NPs is one of the crucial factors influencing lysosomal escape, and we then tested the buffering capacity of NPs by an acid-base titration experiment (Fig. 2D). As expected, PG-PEP showed the strongest buffering in the pH range from 4.0 to 6.0, which indicated that protonation and deprotonation of the tripeptide occurred due to the changes in external hydrogen ion concentration. The buffering capacity of PG-FAPEP was lower than that of PG-PEP due to the presence of hydrophobic folate. PG exhibited the weakest buffering capacity owing to the disappearance of the tripeptide. Thus, PG-PEP and PG-FAPEP could be regarded as buffers in the lysosomal microenvironment and probably benefit from lysosomal escape.

Additionally, the zeta potentials of different NPs were measured at pH 6.8 and pH 5.5, which represented the neutral pH of mucus and cytosolic medium and the acidic pH of lysosomes, respectively (Fig. 2E). PG-PEP and PG-FAPEP were nearly neutrally charged (approximately −4 mV) at pH 6.8, which indicated that they could display great potential for fast diffusion in mucus and cytosol. However, the zeta potentials at pH 5.5 were highly positively charged, mainly due to the protonation of β-carboxyl groups and amine groups of tripepeptide, which might contribute to lysosomal escape.

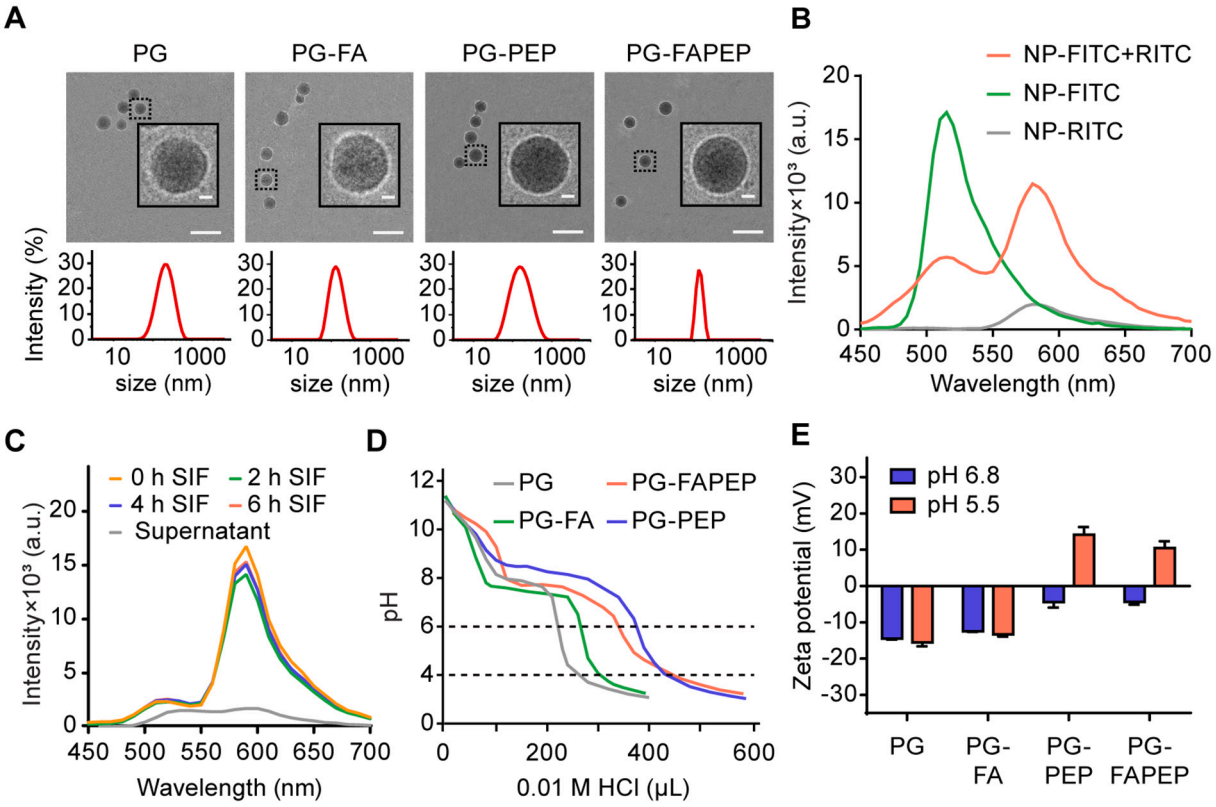

Fig. 2. Preparation and characterization of multifunctional NPs. (A) Cryo-TEM images and size distributions of PG, PG-FA, PG-PEP and PG-FAPEP. Long scale bar: 200 nm, short scale bar: 20 nm. (B) The FRET phenomenon of PG-FAPEP encapsulating FITC and RITC. (C) The stability of PG-FAPEP was evaluated by FRET spectra after incubation with SIF for 6 h. (D) Titration curves of PG, PG-FA, PG-PEP and PG-FAPEP in solution as a function of HCl addition. (E) The zeta potentials of PG, PG-FA, PG-PEP and PG-FAPEP at different pH values.

3.4. Overcoming the mucus barrier

Mucus, a highly viscoelastic and slippery layer with a cross-linked gel-like structure, is one of the major barriers to precluding most pharmaceutics. To check whether the functionalized NPs could obtain improved mucus diffusion capacity, a multiple particle tracking technique was employed to investigate particle diffusion capacities. PG-PEP and PG-FAPEP showed broader diffusion areas than the other NPs (Fig. 3B and C). The MSD of PG-FAPEP was 8.3-fold and 5.5-fold higher than that of PG-FA and PG, respectively, indicating that the tripeptide modification facilitated the diffusion of NPs in mucus. However, PG-FAPEP showed weakened diffusivity compared with PG-PEP, probably resulting from the hydrophobic interaction between folate and mucin. The effective diffusivities (D_{eff}) of NPs at 1 s also indicated the superior mucus diffusion capacities of PG-FAPEP (Fig. 3D). Altogether, these results revealed that PG-FAPEP could move rapidly through mucus and might successfully arrive at the surface of the epithelium (Fig. 3A).

As the pH values differ in the duodenum, jejunum and ileum, we then explored the diffusivities of NPs in mucus collected from different intestinal segments. Consistent with previous investigations, the detected pH of mucus from the duodenum, jejunum and ileum was 6.14, 6.64 and 6.82, respectively (Fig. S7) [43,44]. The mucus diffusion results showed that mucus from everywhere in the small intestine exhibited a limited influence on particle diffusion behaviors (Fig. S8).

3.5. Overcoming the apical membrane barrier

Epithelial cells are the main barrier after the mucus layer. Human colon carcinoma cells (Caco-2) were adopted as monolayers to investigate apical endocytosis capacity, and E12 cells with mucus were used as a model to study the impact of the mucus layer on the internalization of NPs into epithelial cells. The MTT assay suggested that all the NPs were

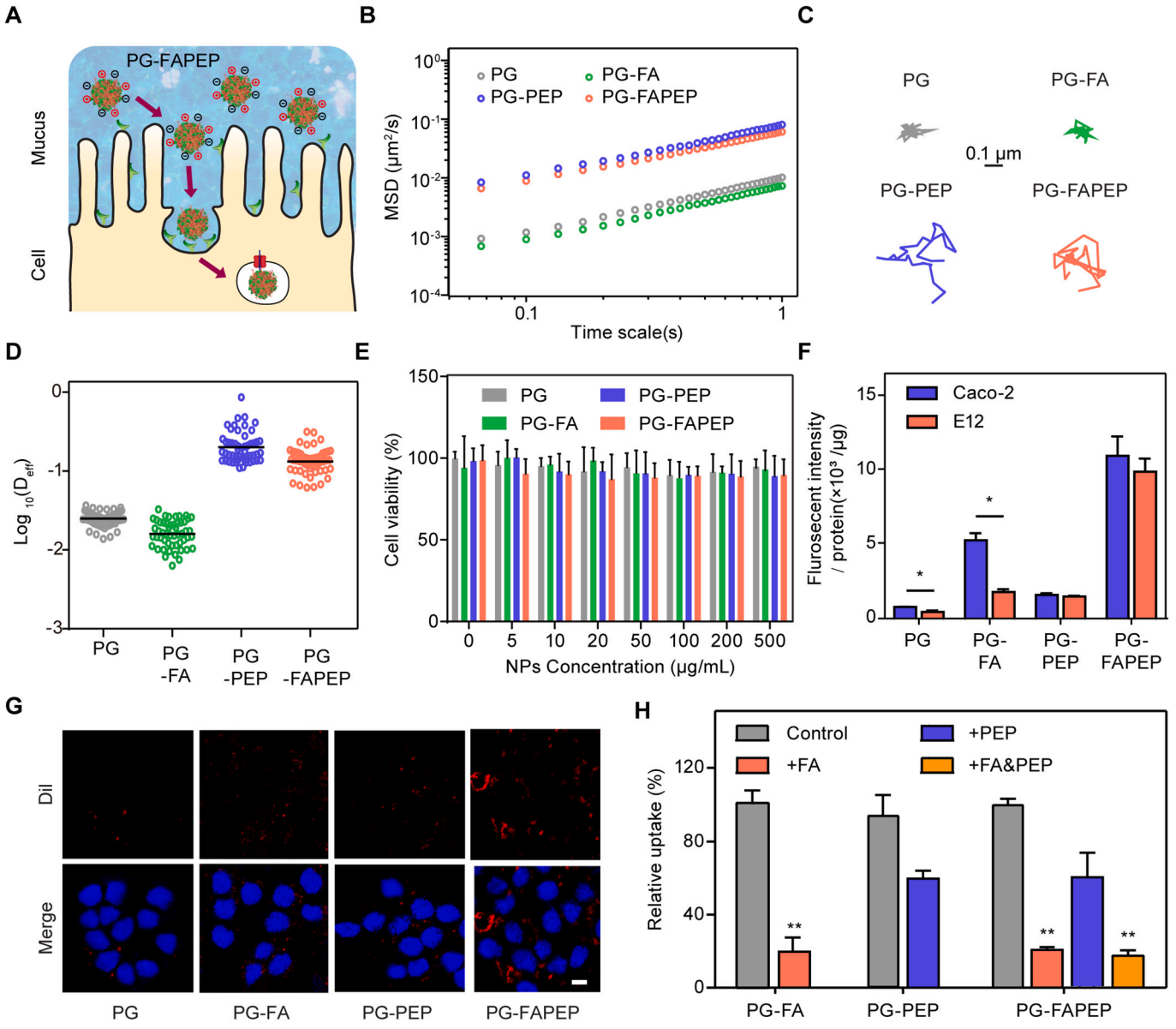

Fig. 3. Mucus diffusion and apical endocytosis. (A) Schematic illustration of mucus diffusion and endocytosis of PG-FAPEP. (B) The MSD of NPs as a function of time scale. $n = 200$. (C) Representative trajectories of NPs in the intestinal mucus at 1 s. (D) Distributions of the logarithms of individual particle effective diffusivities for NPs at a time scale of 1 s. n = 200. (E) The viability of cells incubated with NPs at concentrations from 0 to 500 μg/mL. (F) Quantitative internalization of NPs in E12 cells and Caco-2 cells. $^{*}p < 0.05$. (G) CLSM images of the NPs in Caco-2 cells and E12 cells. Scale bar: 20 μm. (H) Quantitative determination of the cellular uptake amounts of NPs in Caco-2 cells in the presence of excess free folate and tripeptide. $^{**}p < 0.01$.

nontoxic at the tested concentrations (Fig. 3E). The endocytosis efficiency of PG-FAPEP was 6.9-fold higher than that of PG-PEP in Caco-2 cells, indicating that the modification of folate conferred a higher internalization efficiency of PG-FAPEP (Fig. 3F). In E12 cells, the cellular uptake efficiency of PG-FAPEP was 5.5-fold higher than that of the PG-FA group, which is mainly attributed to the enhanced permeation through the mucus layer with the assistance of the tripeptide, leading to the efficient arrival of PG-FAPEP at the surface of cells. Additionally, the internalization amounts of PG-FAs in Caco-2 cells were obviously higher than those in E12 cells according to CLSM images (Fig. 3G), suggesting that PG-FAs were easily trapped by mucus due to hydrophobic folate modification.

To better understand the effects of folate and tripeptide on cellular uptake, the apical endocytosis of PG-FA, PG-PEP and PG-FAPEP was separately analyzed when preincubated with free folate, tripeptide or both. As suggested in Fig. 3H, the internalization of all the NPs was inhibited by the addition of free folate or tripeptide. For PG-FA, apical endocytosis was reduced to merely 21% in the presence of free folate, indicating the important role of folate in cellular internalization. Resulting from a significant inhibition of the free folate or tripeptide, the cellular uptake amounts of PG-FAPEP were decreased to 22% and 61%, respectively. Furthermore, in the presence of both excess folate and tripeptide, an 80% reduction was observed for the apical endocytosis of PG-FAPEP, ensuring the key roles of folate and tripeptide. From these observations, we concluded that both folate and tripeptide modification helped to improve apical endocytosis efficacy, and the effect of folate was stronger than that of tripeptide. Folate receptors were mainly expressed on the apical side of Caco-2 cells, which could guide the efficient internalization of NPs [27]. Thus, the underlying mechanism of enhanced cellular internalization is speculated to be the high affinity of folate on the surface of PG-FAPEP for folate receptors.

3.6. Overcoming the lysosomal degradation barrier

After apical endocytosis, NPs are always encapsulated in lysosomes and then largely degraded [45,46]. Due to the buffering capacity of tripeptide-modified NPs, we expected these NPs to trigger a proton sponge effect to escape lysosomes. Herein, we analyzed the lysosomal escape of NPs using CLSM. After incubation with Caco-2 cells for 0.5 h, almost all the green NPs and red lysosomes were colocalized, and strong

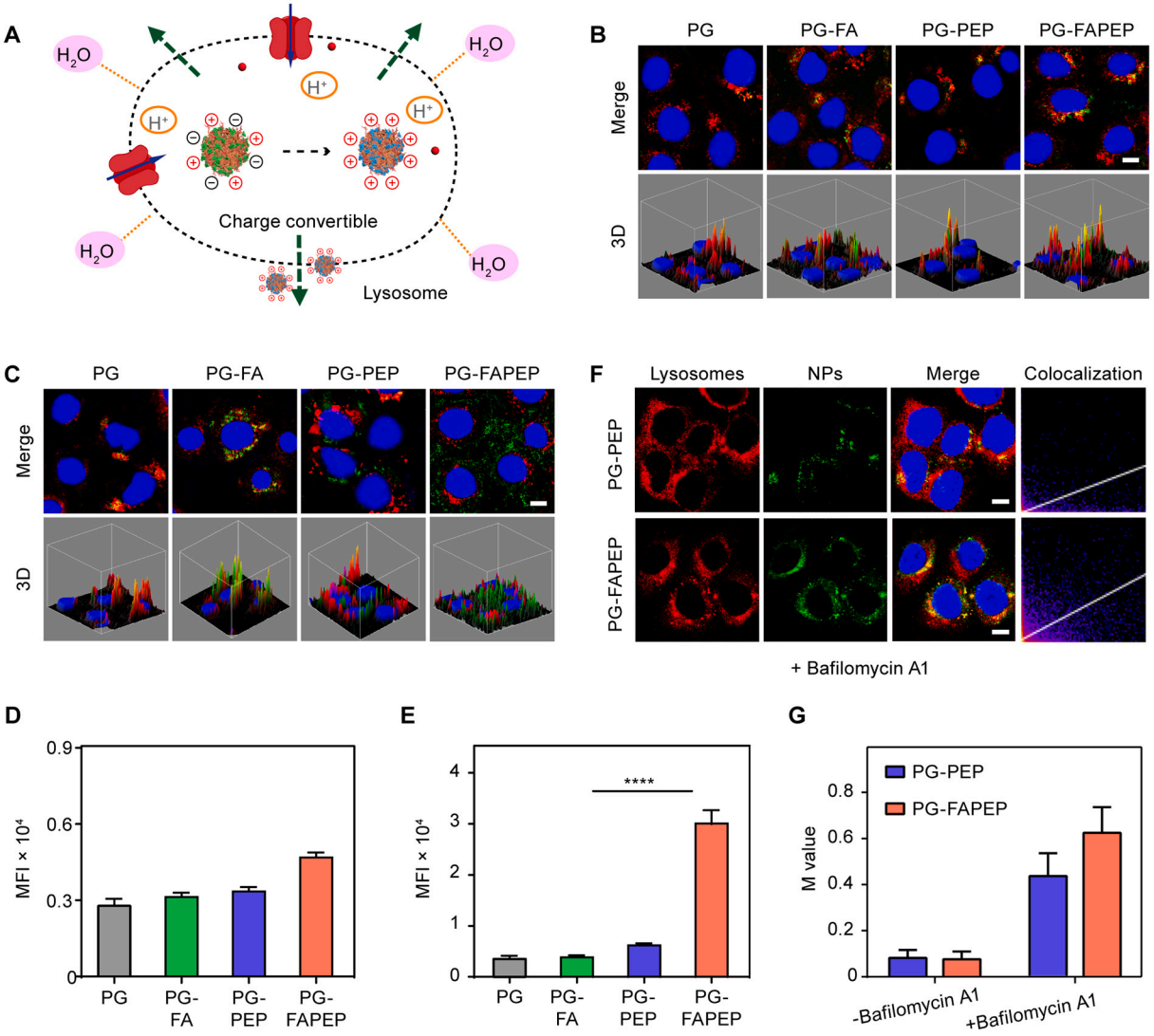

Fig. 4. Lysosomal escape studies of PG-FAPEP. (A) Scheme of the sponge effect induced by charge-convertible NPs. CLSM images of NPs (green) interacting with lysosomes (red) after (B) 0.5 h and (C) 2 h of incubation. Cell nuclei were stained with DAPI (blue). Lysosomes were labeled with LysoTracker DND (red), and FITC-labeled NPs emitted green fluorescence. Scale bar, 10 μm. Quantification analysis of NP escape from lysosomes at (D) 0.5 h and (E) 2 h. $^*p < 0.05$ and $^{****}p < 0.0001$. (F) Lysosomal colocalization images after incubation with bafilomycin A1. (G) Colocalization coefficient with and without bafilomycin A1 incubation. Scale bar, 10 μm. (For interpretation of the references to colour in this figure legend, the reader is referred to the web version of this article.)

yellow fluorescence was clearly observed (Fig. 4B). In contrast, green and red fluorescence displayed less colocalization for PG-FAPEP and PG-PEP after 2 h (Fig. 4C), indicating their excellent lysosomal escape capacities. To intuitively reflect the lysosomal escape capacity of NPs, the obtained fluorescence intensity values were analyzed quantitatively. Most NPs were transported into the lysosomes after 0.5 h of incubation (Fig. 4D). After 2 h of incubation, the escape amounts of PG-FAPEP were 4.8-fold and 7.8-fold higher than those of PG-PEP and PG-FA (Fig. 4E), respectively. To verify the special mechanism by which NPs escape lysosomes, bafilomycin A1 was used to prevent the acidification of lysosomes. As shown in Fig. 4F, after incubation with bafilomycin A1, the majority of tripeptide-modified NPs (PG-PEP and PG-FAPEP) were trapped in lysosomes, and the colocalization efficiency increased up to approximately 60% (Fig. 4G). From all these results, we can conclude that the charge-convertible tripeptide-modified NPs (PG-PEP and PG-FAPEP) could shift the surface charge to be positive *via* protonation when NPs entered lysosomes and then successfully escaped from lysosomes through the proton sponge effect (Fig. 4A).

3.7. Overcoming the intracellular trafficking and basolateral membrane barriers

After escaping lysosomes, NPs encounter a cross-linked gel-like structure of the cytoplasm, which hinders transport toward the basolateral membrane. Therefore, we tracked the movements of NPs in simulated intracellular cytoplasm. The results revealed that PG-FAPEP possessed a high diffusivity within the simulated intracellular medium (Fig. 5A and B), implying that PG-FAPEP could access the basolateral membrane. This finding was also confirmed by observing the distribution of PG-FAPEP in the cell monolayers along the z-axis. As shown in Fig. 5C, a large amount of PG-FAPEP was internalized into cells, and PG-FAPEP was transported deep along the z-axis, efficiently reaching the basolateral side. Thus, PG-FAPEP could successfully conquer the intracellular trafficking barrier.

Owing to the polarity of intestinal epithelia, the basolateral membrane is the last barrier for NPs before entering systemic circulation. As PHT1 could assist the delivery of oligopeptides into systemic circulation, we explored whether PHT1 could guide the exocytosis of PG-FAPEP. A large number of green fluorescent signals were detected, as shown in Fig. 5D, indicating ample expression of PHT1 in Caco-2 cells; at the same time, the colocalization of PHT1 and PG-FAPEP was observed, implying that PG-FAPEP could bind to PHT1 for exocytosis.

We then explored whether PG-FAPEP could be successfully transported across the epithelium. The TEER values of monolayers were measured to ascertain the integrity of cell monolayers during these experiments. No significant decrease was observed in the TEER values among all the groups, revealing that the intracellular pathways were involved in the transportation of NPs (Fig. S9). The transcytosis efficacy of NPs, including PG-FA, PG-PEP and PG-FAPEP, was analyzed quantitatively. The results showed that the apparent permeability (P_{app}) of insulin-loaded PG-FAPEP was approximately 5.0-fold, 4.6-fold and 10.0-fold higher than that of PG-FA, PG-PEP, and free insulin, respectively

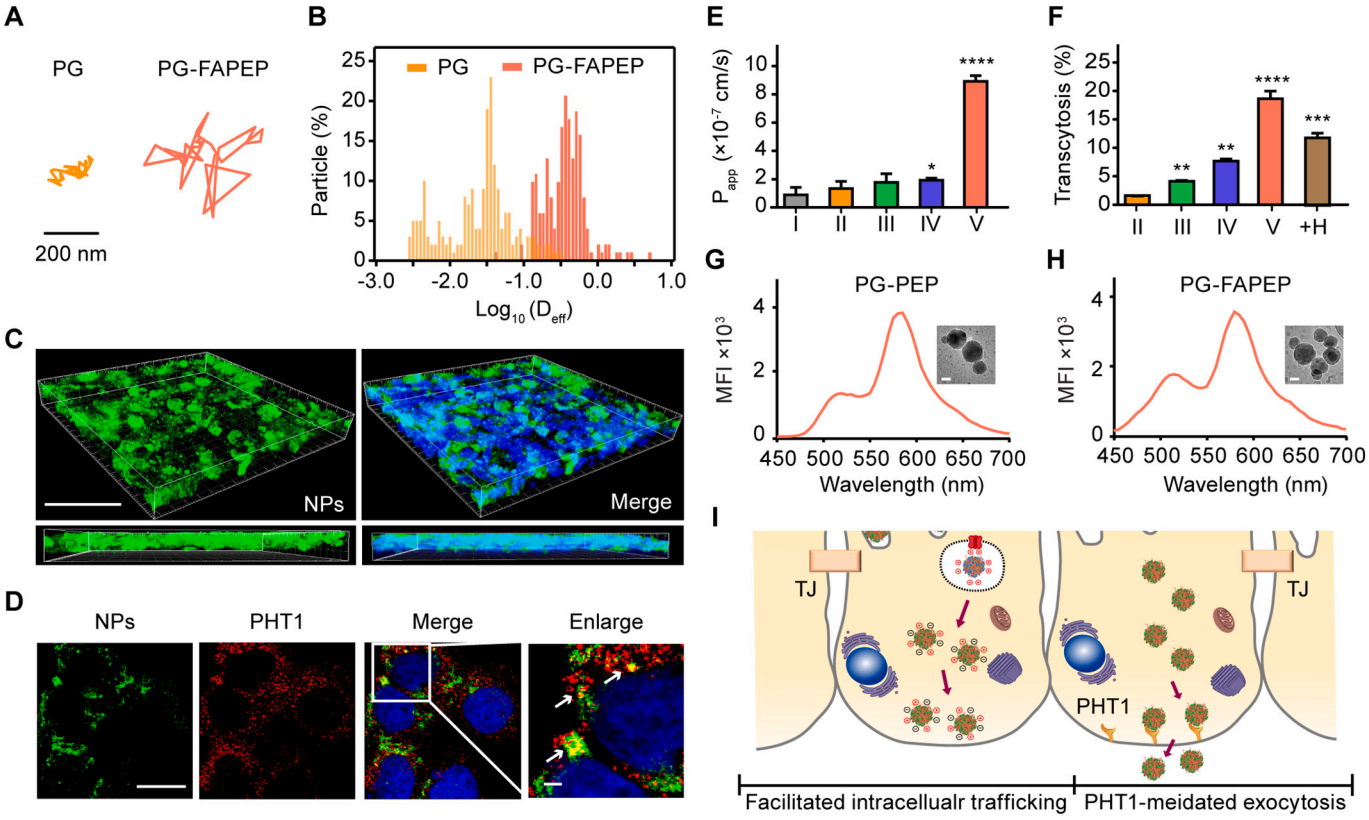

Fig. 5. Intracellular trafficking and basolateral exocytosis studies. (A) Representative trajectories of NPs in stimulated intracellular medium at 1 s. (B) Distributions of the logarithms of individual particle effective diffusivities for NPs at a time scale of 1 s in simulated intracellular cytoplasm. $n = 200$. (C) CLSM 3D images of Caco-2 cell monolayers incubated with PG-FAPEP. Cell nuclei were stained with DAPI. Scale bar, 20 μm. (D) Colocalization of PG-FAPEP with PHT1 after incubation for 2 h. White arrows denote the colocalization of NPs with PHT1 transporters. Scale bar, 20 μm. (E) P_{app} values of FITC-insulin from the different formulations across Caco-2 cell monolayers. I: insulin; II: PG; III: PG-FA; IV: PG-PEP; V: PG-FAPEP. (F) Transcytosis efficacy of insulin-loaded NPs across Caco-2 cell monolayers. II: PG; III: PG-FA; IV: PG-PEP; V: PG-FAPEP; H: His. $^{*}p < 0.05$ and $^{****}p < 0.0001$ compared to the insulin group. FRET phenomenon of PG-PEP (G) and PG-FAPEP (H) collected from the basolateral sides after incubation for 4 h. Insertions: TEM images of NPs collected from the basolateral side of Caco-2 cell monolayers. Scale bar, 50 nm. (I) Illustration of the supposed intracellular trafficking and exocytosis pathways of PG-FAPEP, including fast diffusion in the cellular cytoplasm and PHT1-mediated exocytosis.

(Fig. 5E), indicating that tripeptide and folate modifications could significantly enhance the transcytosis of NPs across the intestinal epithelia. The transcellular efficiencies of PG, PG-FA, PG-PEP, and PG-FAPEP were approximately 1.7%, 4.3%, 8.0% and 19.7%, respectively (Fig. 5F). To detect the integrity of NPs after crossing the basolateral membrane, FRET technology was also applied. The results showed that the FRET phenomenon of PG-FAPEP still occurred, indicating that PG-FAPEP was exocytosed from the basolateral sides in an intact form. For PG-PEP, the FRET phenomenon could be observed to ensure that some intact NPs were exocytosed. Additionally, for the PG-FAPEP and PG-PEP groups, intact NPs with spherical shapes were observed by cryo-TEM images after the transcytosis process (Fig. 5G and H). For the other groups, the FRET phenomenon almost disappeared, suggesting that PG-FA and PG cannot be released as integrity states from the basolateral membrane (Figs. S10 and S11). To verify that the PHT1-mediated pathway was involved in the intracellular transport of PG-FAPEP, histidine (His) was used to inhibit PHT1-mediated secretion. As shown in Fig. 5F, the P_{app} value for PG-FAPEP was significantly decreased in the presence of His, indicating that PG-FAPEP was transported to the bloodstream *via* PHT1-mediated exocytosis. Therefore, the obtained observations revealed that after escaping from lysosomes, PG-FAPEP showed a superior ability to exocytose through the basolateral side. In conclusion, after entering the intracellular environment, PG-FAPEP could escape lysosomes by the proton sponge effect and then exhibited accelerated diffusivity in the cytoplasm, accessing the basolateral side. Finally, PG-FAPEP was exocytosed *via* the PHT1-mediated pathway, sequentially overcoming the multiple absorption barriers (Fig. 5I).

3.8. Real-time visualization of NP transport into intestinal villi

To further investigate the capacity of NPs to overcome oral sequential barriers *in vivo*, intravital two-photon microscopy was used to visualize the real-time absorption of FITC-insulin-loaded NPs. All the obtained movies are listed in the supporting information from Movie S1 to Movie S7. In addition, CLSM was utilized to reflect the distribution of NPs in the intestinal villi. As shown in Fig. 6A and Fig. S12, the

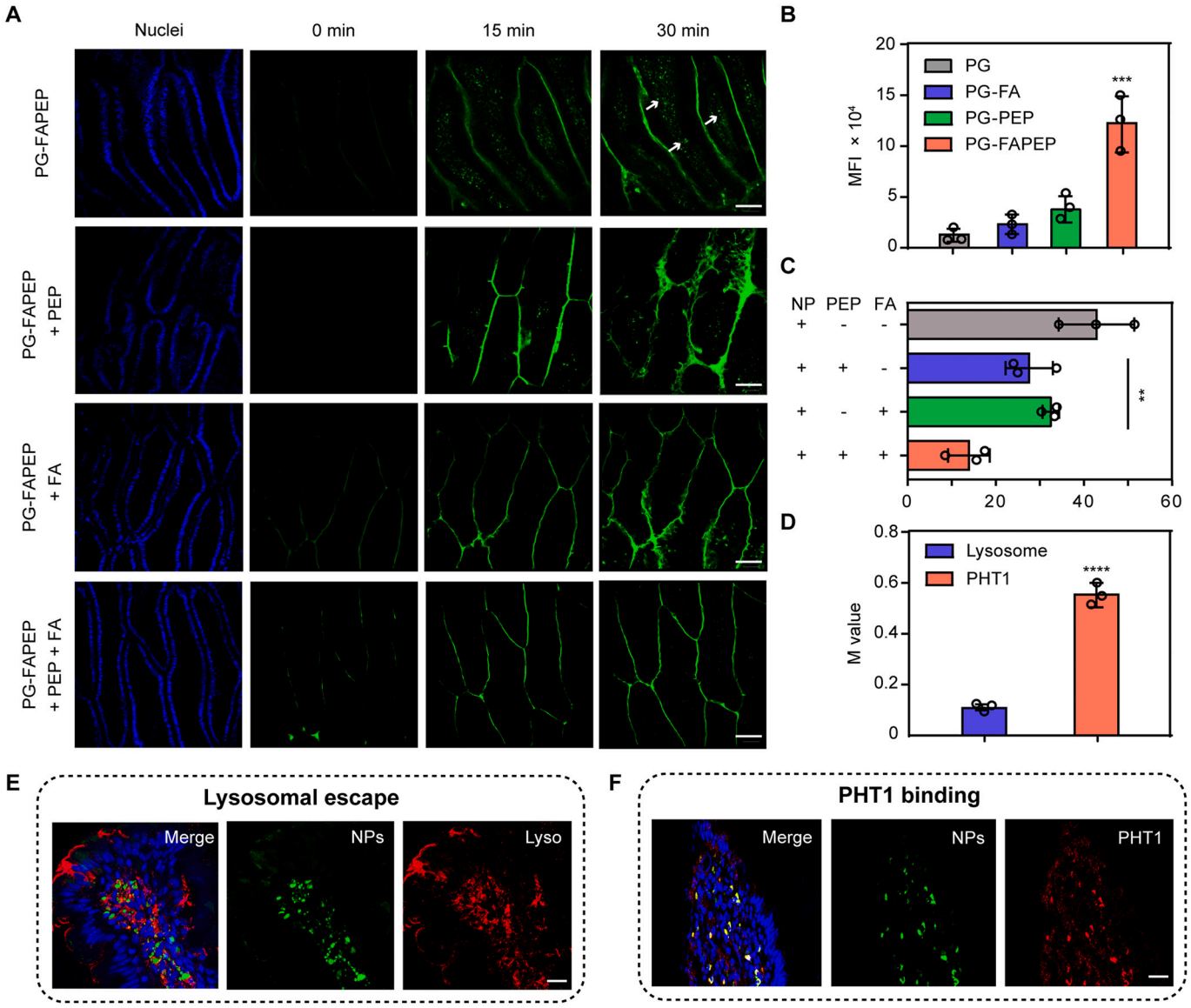

Fig. 6. *Ex vivo* and *in vivo* absorption of NPs. (A) Two-photon microscopy imaging of the absorption of PG-FAPEP into intestinal villi with and without folate and tripeptide. Scale bar: 50 μm. (B) Semiquantitative analysis of the absorption amounts of NPs into intestinal villi. White arrows represented the absorbed NPs. (C) The absorption amounts of PG-FAPEP into intestinal villi when coadministered with folate, tripeptide or both. NP represents PG-FAPEP, PEP represents free tripeptide and FA represents free folate. (D) The colocalization M values of NPs with lysosomes or PHT1. CLSM images of the colocalization of PG-FAPEP with lysosomes (E) or PHT1 (F) in the intestinal villi. Scale bar: 5 μm. Lyso represents lysosome. $^{**}p < 0.01$, $^{***}p < 0.001$ and $^{****}p < 0.0001$.

absorption amounts of FITC-insulin in the villus cavity increased over time. PG-FAPEP exhibited a higher absorption rate, and the highest fluorescence intensity was observed after 30 min. In contrast, little fluorescence was observed for PG at the same time. PG-FA had a similar fluorescence intensity to PG-PEP, which was attributed to the enhanced ability to overcome partial oral sequential barriers with the help of folate or tripeptide. Among these, the charge-convertible tripeptide improved mucus diffusion, at the same time provided the capability of PG-PEP to escape from lysosomes, and folate increased the amounts of PG-FA internalized into the epithelium. The absorption amounts of PG-FAPEP at small intestinal villi were 9.5-fold, 5.8-fold, and 3.5-fold higher than those of PG, PG-FA and PG-PEP, respectively (Fig. 6B).

To study the functions of folate and tripeptide when transported into intestinal villi, PG-FAPEP was incubated with free folate, tripeptide or both. The inner green fluorescence of NPs decreased significantly when pretreated with free folate or tripeptide, which meant that the absorption amount of insulin was dramatically decreased (Fig. 6A, C and Fig. S13). These results demonstrated that folate and tripeptide actually have an outstanding capacity to promote the absorption of PG-FAPEP. Moreover, when the intestinal epithelia were pretreated with both free folate and tripeptide, limited inner green fluorescence was observed, suggesting that there is a joint effect of folate and tripeptide.

We then evaluated the intracellular trafficking of NPs *in vivo* (Fig. 6D-F). CLSM images and the colocalization M values showed nearly no colocalization of lysosomes with PG-FAPEP, ensuring that PG-FAPEP successfully survived degradation. The colocalization of PHT1 with PG-FAPEP was abundant in small intestinal villi, suggesting that PHT1 participated in the absorption of PG-FAPEP. Consistent with the cellular studies, the *in vivo* explorations reflected that PG-FAPEP could prevent degradation from lysosomes and then exocytose *via* the PHT1-mediated pathway for absorption. The obtained results demonstrated that PG-FAPEP has an excellent ability to address sequential oral absorption barriers. All the above phenomena confirmed that the modifications of both folate and tripeptide were vital to overcome intricate barriers for oral delivery of NPs.

3.9. Pharmacodynamic and pharmacokinetic studies in diabetic rats

Finally, diabetic rats were used to study the pharmacodynamics and pharmacokinetics of designed insulin-loaded NPs. To overcome the severely acidic and enzymatic environment in the gastrointestinal tract with high efficiency, HPMCP-coated capsules were used to encapsulate insulin-loaded NPs, which are insoluble in the stomach (pH 1.2) but can be dissolved rapidly in the intestine (pH > 5.5) [47]. Blood glucose at various time points was analyzed in diabetic male SD rats. As shown in Fig. 7A, cINS and cPG exhibited high blood glucose levels, suggesting their poor adsorption capacities. The blood glucose level of the INS s.c. group exhibited a sharp decrease in the first 1 h and continuously decreased for another 1 h, followed by a gradual return to baseline. cPG-FAPEP showed sustained lower blood glucose levels for a long time, and the blood glucose concentration was reduced up to 32% and 50% of the initial level after 4 h and 12 h, respectively. These results suggested that PG-FAPEP could efficiently overcome the sequential absorption barriers to exert excellent hypoglycemic effects.

Blood insulin levels were also determined by ELISA, and the corresponding serum insulin concentrations *vs.* time profile as well as the pharmacokinetic parameters are presented in Fig. 7B and Table S3. A low concentration of insulin was detected in the blood samples of the cINS and cPG groups. The diabetic rats treated with cPG-FA, cPG-PEG and cPG-FAPEP showed a gradual increase in insulin levels in the bloodstream and reached their maximum blood insulin level at 4 h after oral administration. Furthermore, the highest relative oral bioavailability (14.3%) was observed in the cPG-FAPEP group, which was 3.2-fold and 8.4-fold higher than that of the cPG group and cINS group, respectively. The AUC (0−12*h*) for cPG-FAPEP was 219.6 μIU·h·mL^{-1}. At the same time, no significant pathological damage was observed at the intestine in all NP-treated groups from the hematoxylin and eosin (H&E) staining images, demonstrating the outstanding biocompatibility of PG, PG-FA, PG-PEP, and PG-FAPEP (Fig. S14).

At present, the oral administration route provides patient compliance and rapid liver insulinization, leading to adequate insulin delivery. Additionally, insulin delivery by oral administration enters the portal veins natively to imitate the process of endogenous insulin secretion. However, free insulin, directly given by oral administration, is easily degraded by acid and enzymes, leading to poor bioavailability. Charge-convertible tripeptide- and folate-modified PG-FAPEP was designed to protect insulin from degradation and overcome the sequential absorption barriers, in which the tripeptide facilitated mucus penetration, lysosomal escape, intracellular trafficking and basolateral exocytosis, and folate improved cellular uptake, finally significantly increasing bioavailability. Compared with insulin delivered by subcutaneous injection (5 IU/kg), the concentration of insulin in the oral formulation PG-FAPEP (45 IU/kg) was higher to induce a better glycemic effect.

4. Conclusion

In this study, we developed a multifunctional nanoparticle system of PLGA dual-modified with folate and tripeptide that showed excellent

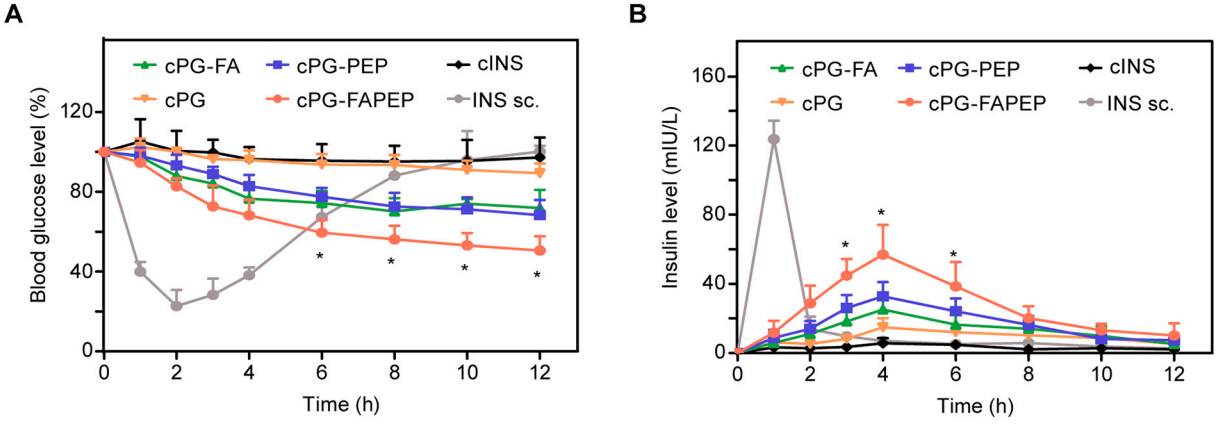

Fig. 7. Pharmacodynamic and pharmacokinetic studies of NPs. (A) Blood glucose levels (%) of the diabetic rats after the oral administration of different insulin-loaded formulations. cPG, cPG-FA, cPG-PEP and cPG-FAPEP were represented as HPMCP-coated capsules encapsulated with insulin-loaded PG, PG-FA, PG-PEP and PG-FAPEP (45 IU/kg), respectively. cINS represents HPMCP-coated capsules loaded with free insulin (45 IU/kg) and trehalose. INS s.c. represents the subcutaneous injection of insulin solution (5 IU/kg). $^{*}p < 0.05$ compared to cPG-PEP group. (B) Serum insulin concentration *vs.* time profiles of diabetic rats. $n = 6$. $^{*}p < 0.05$ compared to cPG-PEP group.

ability to overcome oral sequential absorption barriers for oral insulin delivery. In contrast to conventional NPs coated with dual ligands, PG-FAPEP exhibited accelerated diffusion in the cytoplasm and excellent exocytosis at the basolateral side. Additionally, a clear picture of the PG-FAPEP intracellular trafficking route from apical endocytosis to basolateral side release was depicted completely, including rapid mucus penetration with the help of a charge-convertible tripeptide, enhanced cellular internalization assisted by folate, lysosomal escape, overwhelming pervasion capacity within cytoplasm and PHT1-mediated exocytosis supported by the modified tripeptide. It is worth noting that PG-FAPEP was able to promote transcytosis efficiency across polar epithelial barriers due to the dual targeting moieties (folate and tripeptide) increasing uptake and exocytosis by intracellular ligand-receptor interactions and triggering rapid speed flowing of NPs in cell transport. These results highlight the importance of overcoming the sequential absorption barriers step by step and suggest the potential of PG-FAPEP to improve the oral bioavailability of other protein therapeutics.

Supplementary data to this article can be found online at https://doi.org/10.1016/j.jconrel.2021.11.045.

Author contributions

Conceptualization Y.G., Z.X., M.Y., W.Z., E.A. and L.X.; Data curation Y.G., M.Y., Z.X., W.Z., L.X., and E.A.; Formal analysis Z.X., W.Z., J.L., and F.; Funding acquisition M.Y.; Investigation W.Z. and Z.X.; Methodology N.W.; Project administration A.W.; Resources W.H.; Software C.Z.; Supervision Y.G.; Validation W.H.; Visualization N.W.; Writing - original draft Z.X., M.Y., W.Z. and E.A.; Writing - review & editing Y.G., M.Y., W. Z. and Z.X..

Declaration of Competing Interest

The authors declare no conflicts of interest.

Acknowledgements

The authors would sincerely appreciate the financial support from the National Natural Science Foundation of China (81803445, 82003678 and 82025032), NN-CAS foundation, Science and Technology Commission of Shanghai Municipality (20431900100), National Key R&D Program of China (2020YFE0201700), and the Major International Joint Research Project of Chinese Academy of Sciences (153631KYSB20190020). We would like to thank Jialin Duan for her kind help in obtaining the Cryo-TEM data at the National Center for Protein Science Shanghai. We also thank the National Center for Protein Science Shanghai and express our gratitude to Fengming Liu for her assistance.

References

[1] A.N. Zaykov, J.P. Mayer, R.D. DiMarchi, Pursuit of a perfect insulin, Nat. Rev. Drug Discov. 15 (2016) 425–439.
[2] D.J. Drucker, Advances in oral peptide therapeutics, Nat. Rev. Drug Discov. 19 (2020) 277–289.
[3] S. Malathi, P. Nandhakumar, V. Pandiyan, T.J. Webster, S. Balasubramanian, Novel PLGA-based nanoparticles for the oral delivery of insulin, Int. J. Nanomedicine 10 (2015) 2207–2218.
[4] P. Lundquist, P. Artursson, Oral absorption of peptides and nanoparticles across the human intestine: opportunities, limitations and studies in human tissues, Adv. Drug Deliv. Rev. 106 (2016) 256–276.
[5] S.H. Lee, J.G. Song, H.K. Han, Development of pH-responsive organic-inorganic hybrid nanocomposites as an effective oral delivery system of protein drugs, J. Control. Release 311-312 (2019) 74–84.
[6] O. Veiseh, B.C. Tang, K.A. Whitehead, D.G. Anderson, R. Langer, Managing diabetes with nanomedicine: challenges and opportunities, Nat. Rev. Drug Discov. 14 (2015) 45–57.
[7] S. Sun, N. Liang, X. Gong, W. An, Y. Kawashima, F. Cui, P. Yan, Multifunctional composite microcapsules for oral delivery of insulin, Int. J. Mol. Sci. 18 (2016) 54–67.
[8] S. Seyam, N.A. Nordin, M. Alfatama, Recent progress of chitosan and chitosan derivatives-based nanoparticles: pharmaceutical perspectives of oral insulin delivery, Pharmaceuticals 13 (2020) 307–336.
[9] S. Mitragotri, P.A. Burke, R. Langer, Overcoming the challenges in administering biopharmaceuticals: formulation and delivery strategies, Nat. Rev. Drug Discov. 13 (2014) 655–672.
[10] M. Yu, J. Wang, Y. Yang, C. Zhu, Q. Su, S. Guo, J. Sun, Y. Gan, X. Shi, H. Gao, Rotation-facilitated rapid transport of nanorods in mucosal tissues, Nano Lett. 16 (2016) 7176–7182.
[11] H.J. Kim, S. Ogura, T. Otabe, R. Kamegawa, M. Sato, K. Kataoka, K. Miyata, Fine-tuning of hydrophobicity in amphiphilic polyaspartamide derivatives for rapid and transient expression of messenger RNA directed toward genome engineering in brain, ACS Cent. Sci. 5 (2019) 1866–1875.
[12] G. Sahay, D.Y. Alakhova, A.V. Kabanov, Endocytosis of nanomedicines, J. Control. Release 145 (2010) 182–195.
[13] H. Gao, H. Takemoto, Q. Chen, M. Naito, H. Uchida, X. Liu, K. Miyata, K. Kataoka, Regulated protonation of polyaspartamide derivatives bearing repeated aminoethylene side chains for efficient intracellular siRNA delivery with minimal cytotoxicity, Chem. Commun. 51 (2015) 3158–3161.
[14] B. He, P. Lin, Z. Jia, W. Du, W. Qu, L. Yuan, W. Dai, H. Zhang, X. Wang, J. Wang, X. Zhang, Q. Zhang, The transport mechanisms of polymer nanoparticles in Caco-2 epithelial cells, Biomaterials 34 (2013) 6082–6098.
[15] W. Fan, D. Xia, Q. Zhu, X. Li, S. He, C. Zhu, S. Guo, L. Hovgaard, M. Yang, Y. Gan, Functional nanoparticles exploit the bile acid pathway to overcome multiple barriers of the intestinal epithelium for oral insulin delivery, Biomaterials 151 (2018) 13–23.
[16] M. Lopes, N. Shrestha, A. Correia, M.A. Shahbazi, B. Sarmento, J. Hirvonen, F. Veiga, R. Seica, A. Ribeiro, H.A. Santos, Dual chitosan/albumin-coated alginate/dextran sulfate nanoparticles for enhanced oral delivery of insulin, J. Control. Release 232 (2016) 29–41.
[17] C. Twarog, S. Fattah, J. Heade, S. Maher, E. Fattal, D.J. Brayden, Intestinal permeation enhancers for oral delivery of macromolecules: A comparison between salcaprozate sodium (SNAC) and sodium caprate (C10), Pharmaceutics 11 (2019) 78.
[18] B. Xu, G. Jiang, W. Yu, D. Liu, Y. Liu, X. Kong, J. Yao, Preparation of poly(lactic-co-glycolic acid) and chitosan composite nanocarriers via electrostatic self assembly for oral delivery of insulin, Mater. Sci. Eng. C Mater. Biol. Appl. 78 (2017) 420–428.
[19] H. Cabral, K. Miyata, A. Kishimura, Nanodevices for studying nano-pathophysiology, Adv. Drug Deliv. Rev. 74 (2014) 35–52.
[20] A. Gedawy, J. Martinez, H. Al-Salami, C.R. Dass, Oral insulin delivery: existing barriers and current counter-strategies, J. Pharm. Sci. 70 (2018) 197–213.
[21] H. Wang, S. Ding, Z. Zhang, L. Wang, Y. You, Cationic micelle: A promising nanocarrier for gene delivery with high transfection efficiency, J. Gene Med. 21 (2019) 1–16.
[22] X. Zhang, D. Chen, S. Ba, J. Zhu, J. Zhang, W. Hong, X. Zhao, H. Hu, M. Qiao, Poly (l-histidine) based triblock copolymers: pH induced reassembly of copolymer micelles and mechanism underlying endolysosomal escape for intracellular delivery, Biomacromolecules 15 (2014) 4032–4045.
[23] M. Yu, W. Song, F. Tian, Z. Dai, Q. Zhu, E. Ahmad, S. Guo, C. Zhu, H. Zhong, Y. Yuan, T. Zhang, X. Yi, X. Shi, Y. Gan, H. Gao, Temperature- and rigidity-mediated rapid transport of lipid nanovesicles in hydrogels, Proc. Natl. Acad. Sci. U. S. A. 116 (2019) 5362–5369.
[24] D. Nie, Z. Dai, J. Li, Y. Yang, Z. Xi, J. Wang, W. Zhang, K. Qian, S. Guo, C. Zhu, R. Wang, Y. Li, M. Yu, X. Zhang, X. Shi, Y. Gan, Cancer-cell-membrane-coated nanoparticles with a yolk-shell structure augment cancer chemotherapy, Nano Lett. 20 (2019) 936–946.
[25] J. Fels, S.N. Orlov, R. Grygorczyk, The hydrogel nature of mammalian cytoplasm contributes to osmosensing and extracellular pH sensing, Biophys. J. 96 (2009) 4276–4285.
[26] D. Yang, D. Liu, H. Deng, J. Zhang, M. Qin, L. Yuan, X. Zou, B. Shao, H. Li, W. Dai, H. Zhang, X. Wang, B. He, X. Tang, Q. Zhang, Transferrin functionization elevates transcytosis of nanogranules across epithelium by triggering polarity-associated transport flow and positive cellular feedback loop, ACS Nano 13 (2019) 5058–5076.
[27] E. Roger, S. Kalscheuer, A. Kirtane, B.R. Guru, A.E. Grill, J. Whittum-Hudson, J. Panyam, Folic acid functionalized nanoparticles for enhanced oral drug delivery, Mol. Pharm. 9 (2012) 2103–2110.
[28] A.K. Agrawal, D. Urimi, H. Harde, V. Kushwah, S. Jain, Folate appended chitosan nanoparticles augment the stability, bioavailability and efficacy of insulin in diabetic rats following oral administration, RSC Adv. 5 (2015) 105179–105193.
[29] F. Song, Y. Hu, Y. Wang, D.E. Smith, H. Jiang, Functional characterization of human peptide/histidine transporter 1 in stably transfected MDCK cells, Mol. Pharm. 15 (2018) 385–393.
[30] L. Zhu, L. Lu, S. Wang, J. Wu, J. Shi, T. Yan, C. Xie, Q. Li, M. Hu, Z. Liu, Oral absorption basics: Pathways and physicochemical and biological factors affecting absorption, in: Yihong Qiu, Geoff G.Z. Zhang (Eds.), Developing Solid Oral Dosage Forms, Elsevier Inc., Guangdong, 2017, pp. 297–329.
[31] J. Park, J.U. Choi, K. Kim, Y. Byun, Bile acid transporter mediated endocytosis of oral bile acid conjugated nanocomplex, Biomaterials 147 (2017) 145–154.
[32] L. Kou, Q. Yao, M. Sun, C. Wu, J. Wang, Q. Luo, G. Wang, Y. Du, Q. Fu, J. Wang, Z. He, V. Ganapathy, J. Sun, Cotransporting ion is a trigger for cellular endocytosis of transporter-targeting nanoparticles: A case study of high-efficiency SLC22A5 (OCTN2)-mediated carnitine-conjugated nanoparticles for oral delivery of therapeutic drugs, Adv. Healthc. Mater. (2017) 1700165.

[33] L. Kou, Y.D. Bhutia, Q. Yao, Z. He, J. Sun, V. Ganapathy, Transporter-guided delivery of nanoparticles to improve drug permeation across cellular barriers and drug exposure to selective cell types, Front. Pharmacol. 9 (2018) 00027.
[34] B. Sarmento, S. Martins, D. Ferreira, E.B. Souto, Oral insulin delivery by means of solid lipid nanoparticles, Int. J. Nanomedicine 2 (2007) 743–749.
[35] A. White, P. Handler, E.L. Smith, Principles of biochemistry, Acad. Med. 39 (1964) 1136.
[36] X. Zhu, J. Wu, W. Shan, Z. Zhou, M. Liu, Y. Huang, Sub-50 nm nanoparticles with biomimetic surfaces to sequentially overcome the mucosal diffusion barrier and the epithelial absorption barrier, Adv. Funct. Mater. 26 (2016) 2728–2738.
[37] M. Ou, R. Xu, S.H. Kim, D.A. Bull, S.W. Kim, A family of bioreducible poly(disulfide amine)s for gene delivery, Biomaterials 30 (2009) 5804–5814.
[38] C. Maderuelo, J.M. Lanao, A. Zarzuelo, Enteric coating of oral solid dosage forms as a tool to improve drug bioavailability, Eur. J. Pharm. Sci. 138 (2019), 105019.
[39] Z.M. Wu, L. Ling, L.Y. Zhou, X.D. Guo, W. Jiang, Y. Qian, K.Q. Luo, L.J. Zhang, Novel preparation of PLGA/HP55 nanoparticles for oral insulin delivery, Nanoscale Res. Lett. 7 (2012) 299.
[40] X. Li, J. Qi, Y. Xie, X. Zhang, S. Hu, Y. Xu, Y. Lu, W. Wu, Nanoemulsions coated with alginate/chitosan as oral insulin delivery systems: preparation, characterization, and hypoglycemic effect in rats, Int. J. Nanomedicine 8 (2013) 23–32.
[41] Y. Ping, D. Ding, R.A.N.S. Ramos, H. Mohanram, K. Deepankumar, J. Gao, G. Tang, A. Miserez, Supramolecular β-sheets stabilized protein nanocarriers for drug delivery and gene transfection, ACS Nano 11 (2017) 4528–4541.
[42] G. Ru, L. Han, J. Qing, J. Sheng, R. Li, M. Qiu, J. Wang, Effects of borneol on the pharmacokinetics of 9-nitrocamptothecin encapsulated in PLGA nanoparticles with different size via oral administration, Drug Deliv. 23 (2016) 3417–3423.
[43] E.L. McConnell, A.W. Basit, S. Murdan, Measurements of rat and mouse gastrointestinal pH, fluid and lymphoid tissue, and implications for in-vivo experiments, J. Pharm. Sci. 60 (2008) 63–70.
[44] S.G. Nugent, D. Kumar, D.S. Rampton, D.F. Evans, Intestinal luminal pH in inflammatory bowel disease: possible determinants and implications for therapy with aminosalicylates and other drugs, Gut 48 (2001) 571–577.
[45] Y. Xu, Y. Zheng, L. Wu, X. Zhu, Z. Zhang, Y. Huang, Novel solid lipid nanoparticle with endosomal escape function for oral delivery of insulin, ACS Appl. Mater. Interfaces 10 (2018) 9315–9324.
[46] P. Fonte, F. Araujo, S. Reis, B. Sarmento, Oral insulin delivery: how far are we? J. Diabetes Sci. Technol. 7 (2013) 520–531.
[47] Z.M. Wu, L. Zhou, X.D. Guo, W. Jiang, L. Ling, Y. Qian, K.Q. Luo, L.J. Zhang, HP55-coated capsule containing PLGA/RS nanoparticles for oral delivery of insulin, Int. J. Pharm. 425 (2012) 1–8.